AIP | The Journal of Chemical Physics

On the widths of Stokes lines in Raman scattering from molecules adsorbed at metal surfaces and in molecular conduction junctions

Yi Gao, Michael Galperin, and Abraham Nitzan

Citation: The Journal of Chemical Physics **144**, 244114 (2016); doi: 10.1063/1.4954912
View online: http://dx.doi.org/10.1063/1.4954912
View Table of Contents: http://scitation.aip.org/content/aip/journal/jcp/144/24?ver=pdfcov
Published by the AIP Publishing

On the widths of Stokes lines in Raman scattering from molecules adsorbed at metal surfaces and in molecular conduction junctions

Yi Gao,[1,a)] Michael Galperin,[1,b)] and Abraham Nitzan[2,c)]
[1]*Department of Chemistry and Biochemistry, University of California San Diego, La Jolla, California 92093, USA*
[2]*Department of Chemistry, University of Pennsylvania, Philadelphia, Pennsylvania 19104, USA and School of Chemistry, Tel Aviv University, Tel Aviv 69978, Israel*

(Received 25 March 2016; accepted 15 June 2016; published online 29 June 2016)

Within a generic model we analyze the Stokes linewidth in surface enhanced Raman scattering (SERS) from molecules embedded as bridges in molecular junctions. We identify four main contributions to the off-resonant Stokes signal and show that under zero voltage bias (a situation pertaining also to standard SERS experiments) and at low bias junctions only one of these contributions is pronounced. The linewidth of this component is determined by the molecular vibrational relaxation rate, which is dominated by interactions with the essentially bosonic thermal environment when the relevant molecular electronic energy is far from the metal(s) Fermi energy(ies). It increases when the molecular electronic level is close to the metal Fermi level so that an additional vibrational relaxation channel due to electron-hole (eh) exciton in the molecule opens. Other contributions to the Raman signal, of considerably broader linewidths, can become important at larger junction bias. *Published by AIP Publishing.* [http://dx.doi.org/10.1063/1.4954912]

I. INTRODUCTION

Molecular optoelectronics is an active field of research made possible by advances in laser technology and nanofabrication.[1] The possibility to conduct optical measurements in open non-equilibrium nano-systems resulted in the appearance of new diagnostic tools, and offers a route to optical control schemes such as switching in molecular electronics devices. Standard observables of optical spectroscopy can yield new information when monitored in open current-carrying molecular junctions. For example, current-induced fluorescence[2,3] yields information on molecular resonances in the non-equilibrium system and makes imaging at submolecular resolution feasible, while the intensity of the emitted light corresponds to charge current noise at optical frequencies[4,5] and can yield information on fast voltage transients at the tunnel junction.[6] Raman spectroscopy of current-carrying junctions can serve as a diagnostic tool similar to inelastic tunneling spectroscopy, and as an indicator for current-induced heating of electronic and vibrational degrees of freedom.[7–9] (Possible pitfalls of such characterization were discussed theoretically.[10,11]) Recently, measurements of *dc* current and/or noise in response to laser pulse pair sequence were suggested as a variant of pump-probe spectroscopy for molecular junctions capable of providing information on intra-molecular dynamics at sub-picosecond time scale.[12,13]

As noted above, the ability to characterize vibrational structure of a molecular device makes Raman scattering similar to inelastic electron tunneling spectroscopy (IETS). The corresponding spectra are characterized by their peak positions and heights, as well as lineshapes and linewidths. In addition to standard peaks, rich IETS lineshape features caused by interference between elastic and inelastic scattering channels are known.[14,15] Similar interference features in Raman scattering were recently discussed.[16] The dependence of (resonant) IETS spectra on gate and source-drain biases was measured and discussed.[17–19] It appears to primarily manifest the sensitivity of molecular normal modes to the molecule charging state.[20,21] Similarly, a shift in the frequencies of Stokes lines with bias was observed[9,22] and was shown to result at least partly from the voltage dependence of the charge on the molecule.[23–26] Finally, the linewidths of IETS signals were studied both experimentally[27] and theoretically[28] and were shown to be dominated by the strength of electron-phonon interactions. No such study has been done so far for Raman scattering from molecular junctions.

The present paper focuses on the latter issue: we identify the main contribution to the observed Raman intensity and analyze, using a generic model, the non-monotonic dependence of the Stokes linewidth on the gate and bias potentials. In Section II we introduce our model for an illuminated molecular junction as well as our calculation methodology for off-resonant Raman scattering from this system. Section III presents our results and Section IV concludes.

II. MODEL AND METHOD

We consider a junction comprised of a molecule coupled to two metallic contacts, L and R, each at its own equilibrium. The molecule is represented by two electronic levels (ground, ε_g, and excited, ε_x, states)[29] and a molecular vibration, taken

[a)]yig057@ucsd.edu
[b)]migalperin@ucsd.edu
[c)]nitzan@post.tau.ac.il

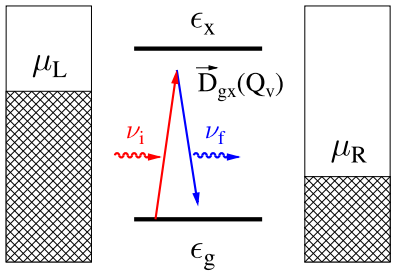

FIG. 1. A sketch of the model for off-resonant Raman scattering in a junction. The junction consists of a molecule (modeled by two-level system—ε_g and ε_x) coupled to two metallic contacts each characterized by its own electrochemical potential μ_L and μ_R. Off-resonant Raman signal originates from the dependence of the transition dipole moment $\vec{D}_{gx}$ on vibrational coordinate Q_v. ν_i and ν_f are incoming and outgoing photon frequencies.

harmonic of frequency ω_v, linearly coupled to the levels populations (a Holstein-type model). The junction is subjected to an external radiation field, represented by a set of quantum harmonic modes $\{\nu_\alpha\}$ (see sketch in Fig. 1). One of these modes, of frequency ν_i, represents the incident mode that pumps the system. All other modes, $\{\nu_f\}$, are taken to be vacant. The Hamiltonian is

$$\hat{H} = \hat{H}_0 + \hat{H}_{rad} + \hat{V}, \tag{1}$$

where $\hat{H}_0$ represents the dark junction, $\hat{H}_{rad}$ is Hamiltonian of the radiation field, and $\hat{V}$ is the molecule-field coupling. Explicitly

$$\begin{aligned}\hat{H}_0 = &\sum_{m=g,x} \varepsilon_m \hat{n}_m + \omega_v \hat{v}^\dagger \hat{v} + \sum_k \varepsilon_k \hat{n}_k + \sum_\beta \omega_\beta \hat{b}_\beta^\dagger \hat{b}_\beta \\ &+ \sum_{k,m} \left(V_{km} \hat{c}_k^\dagger \hat{d}_m + H.c. \right) + \sum_{m=g,x} M_m \hat{Q}_v \hat{n}_m \\ &+ \sum_\beta V_\beta^{th} \hat{Q}_\beta \hat{Q}_v, \end{aligned} \tag{2}$$

$$\hat{H}_{rad} = \sum_{\alpha \in i\{f\}} \nu_\alpha \hat{a}_\alpha^\dagger \hat{a}_\alpha, \tag{3}$$

$$\hat{V} = \sum_\alpha \left(U_{\alpha D}(\hat{Q}_v)\, \hat{a}_\alpha^\dagger \hat{D} + H.c. \right). \tag{4}$$

Here $\hat{d}_m^\dagger$ ($\hat{d}_m$) and $\hat{c}_k^\dagger$ ($\hat{c}_k$) create (annihilate) electrons in the molecular level m and state k of the metal contacts, respectively. $\hat{n}_m = \hat{d}_m^\dagger \hat{d}_m$ and $\hat{n}_k = \hat{c}_k^\dagger \hat{c}_k$ are the corresponding electron number operators for states $m\,(=g,x)$ of the molecule and k of the contacts. $\hat{D}^\dagger = \hat{d}_x^\dagger \hat{d}_g$ and $\hat{D} = \hat{d}_g^\dagger \hat{d}_x$ are molecular excitation and de-excitation operators. $\hat{v}^\dagger$ ($\hat{v}$) and $\hat{b}_\beta^\dagger$ ($\hat{b}_\beta$) create (annihilate) vibrational quanta in the molecule and mode β of the thermal bath, respectively. $\hat{Q}_v = \hat{v} + \hat{v}^\dagger$ and $\hat{Q}_\beta = \hat{b}_\beta + \hat{b}_\beta^\dagger$ are the oscillators position operators. The thermal bath accounts for energy dissipation due to coupling of the primary vibrational mode to other vibrational modes of the molecule and environment, i.e., other molecules, phonons in contacts, etc. $\hat{a}_\alpha^\dagger$ ($\hat{a}_\alpha$) creates (destroys) a photon in the mode α of radiation field. Note that this model contains two interactions that can cause inelastic light scattering. First is the dependence of the molecule-field coupling U on the vibrational coordinate. The other is the polaronic coupling term in Eq. (2) whose importance is measured by the electron-vibration coupling M.

Following Refs. 30 and 31 and focusing on the low voltage bias regime, we consider only "normal Raman" scattering, i.e., a process where the initial molecular state is its ground state.[32] Raman scattering is a coherent process of fourth order in the matter-radiation field coupling (two orders correspond to the outgoing photon, blue line in Fig. 1, and two orders correspond to the incoming photon, red line in Fig. 1). Explicit steady-state expression for the "normal Raman" scattering from the initial mode i to a final mode f of the radiation field is (see Ref. 31 for details)

$$\begin{aligned} J_{i\to f} = &\int_{-\infty}^{+\infty} d(t'-t) \int_{-\infty}^{0} d(t_1-t) \int_{-\infty}^{0} d(t_2-t') \\ &\times e^{-i\nu_f(t'-t)}\, e^{-i\nu_i(t_1-t_2)} \left\langle \hat{U}_{iD}(t_2)\hat{D}(t_2) \right. \\ &\left. \times \hat{U}_{Df}(t')\hat{D}^\dagger(t')\, \hat{U}_{fD}(t)\hat{D}(t)\, \hat{U}_{Di}(t_1)\hat{D}^\dagger(t_1) \right\rangle, \end{aligned} \tag{5}$$

where $\hat{U}_{\alpha D} \equiv U_{\alpha D}(\hat{Q}_v)$. Here ν_i and ν_f are frequencies of incoming and outgoing photons, operators are written in the Heisenberg picture and $\langle \ldots \rangle \equiv \mathrm{Tr}[\ldots \hat{\rho}_0]$ is a quantum-mechanical and statistical average with the initial ($t \to -\infty$) density operator of the model. As in standard treatments, we expand the molecule-field coupling to linear terms in Taylor series in the molecular vibrational displacement

$$U_{\alpha D}(\hat{Q}_v) \approx U_{\alpha D}^{(0)} + U_{\alpha D}^{(1)}\, \hat{Q}_v. \tag{6}$$

Depending on the combination of molecule-field coupling terms ($U_{\alpha D}^{(0)}$ or $U_{\alpha D}^{(1)}\hat{Q}_v$) in the expression (5) one gets contributions to vibrational and electronic Raman (Rayleigh) scatterings. For example, substituting only $U_{\alpha D}^{(0)}$ in place of all molecule-field couplings in Eq. (5) yields the pure electronic Raman contribution discussed in Refs. 10 and 11. Here we focus on the vibrational Raman scattering, whose lowest order contribution comes from terms that are second order in the coupling to the molecular vibration. Such terms will be of order $\left(U^{(1)}\right)^2$. After collecting all such contributions to the vibrational Raman, we (a) separate vibrational and electronic degrees of freedom (i.e., neglect vibration-induced electronic correlations) and (b) neglect electronic correlation between ground and excited states of the molecule assuming that the energy gap between them is much larger than the widths associated with their coupling to the contacts. We focus on off-resonant Raman scattering and restrict our consideration to gate voltages that keep the upper electronic level above the lead chemical potentials (so it is essentially unpopulated). Under these approximations the explicit expression becomes

$$\begin{aligned} J_{\nu_i\to\nu_f} = &\rho(\nu_i)\Delta\nu_i\, \rho(\nu_f)\Delta\nu_f \mathrm{Re} \int \frac{dE_{g1}}{2\pi} \int \frac{dE_{g2}}{2\pi} \int \frac{dE_{x1}}{2\pi} \int \frac{dE_{x2}}{2\pi} \\ &\times \left\{ iD^>(\nu_{if}) G_g^<(E_{g1}) G_g^<(E_{g2}) G_x^>(E_{x1}) G_x^>(E_{x2}) \frac{2\, U_{iD}^{(0)} U_{Df}^{(1)} U_{fD}^{(0)} U_{Di}^{(1)} + U_{iD}^{(1)} U_{Df}^{(0)} U_{fD}^{(0)} U_{Di}^{(1)} + U_{iD}^{(0)} U_{Df}^{(1)} U_{fD}^{(1)} U_{Di}^{(0)}}{(\nu_f - E_{x2} + E_{g2} + i\delta)(\nu_i - E_{x1} + E_{g1} - i\delta)} \right. \end{aligned} \tag{7a}$$

$$-iD^{>}(\nu_{if}-E_{g21})G_g^{<}(E_{g1})G_g^{>}(E_{g2})G_x^{>}(E_{x1})G_x^{>}(E_{x2})\Big(\frac{2\,U_{iD}^{(0)}U_{Df}^{(1)}U_{fD}^{(0)}U_{Di}^{(1)}}{(\nu_f-E_{x2}+E_{g2}+i\delta)(\nu_i-E_{x1}+E_{g1}-i\delta)}$$
$$+\frac{U_{iD}^{(1)}U_{Df}^{(0)}U_{fD}^{(0)}U_{Di}^{(1)}}{(\nu_f-E_{x2}+E_{g2}+i\delta)(\nu_f-E_{x1}+E_{g2}-i\delta)}+\frac{U_{iD}^{(0)}U_{Df}^{(1)}U_{fD}^{(1)}U_{Di}^{(0)}}{(\nu_i-E_{x2}+E_{g1}+i\delta)(\nu_i-E_{x1}+E_{g1}-i\delta)}\Big) \tag{7b}$$

$$-iD^{>}(\nu_{if}-E_{x21})G_g^{<}(E_{g1})G_g^{<}(E_{g2})G_x^{<}(E_{x1})G_x^{>}(E_{x2})\Big(\frac{2\,U_{iD}^{(0)}U_{Df}^{(1)}U_{fD}^{(0)}U_{Di}^{(1)}}{(\nu_f-E_{x1}+E_{g2}+i\delta)(\nu_i-E_{x2}+E_{g1}-i\delta)}$$
$$+\frac{U_{iD}^{(1)}U_{Df}^{(0)}U_{fD}^{(0)}U_{Di}^{(1)}}{(\nu_f-E_{x1}+E_{g2}+i\delta)(\nu_f-E_{x1}+E_{g1}-i\delta)}+\frac{U_{iD}^{(0)}U_{Df}^{(1)}U_{fD}^{(1)}U_{Di}^{(0)}}{(\nu_i-E_{x2}+E_{g2}+i\delta)(\nu_i-E_{x2}+E_{g1}-i\delta)}\Big) \tag{7c}$$

$$-iD^{>}(\nu_{if}-E_{x21}-E_{g21})G_g^{<}(E_{g1})G_g^{>}(E_{g2})G_x^{<}(E_{x1})G_x^{>}(E_{x2})\Big(\frac{2\,U_{iD}^{(0)}U_{Df}^{(1)}U_{fD}^{(0)}U_{Di}^{(1)}}{(\nu_f-E_{x1}+E_{g2}+i\delta)(\nu_i-E_{x2}+E_{g1}-i\delta)}$$
$$+\frac{U_{iD}^{(1)}U_{Df}^{(0)}U_{fD}^{(0)}U_{Di}^{(1)}}{|\nu_f-E_{x1}+E_{g2}+i\delta|^2}+\frac{U_{iD}^{(0)}U_{Df}^{(1)}U_{fD}^{(1)}U_{Di}^{(0)}}{|\nu_i-E_{x2}+E_{g1}+i\delta|^2}\Big)\Big\}. \tag{7d}$$

Here $\nu_{if}=\nu_i-\nu_f$, $E_{m21}=E_{m2}-E_{m1}$ $(m=g,x)$, $G_m^{>/</r}(E)$ and $D^{>}(\omega)$ are Fourier transforms of the greater/lesser/retarded projections of the single electron Green function and the greater projection of the phonon Green function, respectively (see the Appendix for details)

$$G_m(\tau,\tau')=-i\langle T_c\,\hat{d}_m(\tau)\,\hat{d}_m^{\dagger}(\tau')\rangle, \tag{8}$$
$$D(\tau,\tau')=-i\langle T_c\,\hat{Q}_v(\tau)\,\hat{Q}_v(\tau')\rangle, \tag{9}$$

where T_c is the contour ordering operator. $\rho(\nu)\equiv\nu^2/\pi^2c^3$ is the density of optical modes.

Next, some simplification can be made by invoking the reasonable assumption that the molecule-contacts coupling is much larger than the molecule-radiation field coupling as well as the electron-phonon interaction. Under this assumption we can disregard the latter interactions in the expressions for the electronic Green functions, taking the forms that correspond to a molecule coupled to the two metal leads,

$$G_m^r(E)=\Big[E-\varepsilon_m+i\Gamma_m/2\Big]^{-1}, \tag{10}$$
$$G_m^{<}(E)=i\frac{\Gamma_m^L f_L(E)+\Gamma_m^R f_R(E)}{(E-\varepsilon_m)^2+(\Gamma_m/2)^2}, \tag{11}$$
$$G_m^{>}(E)=-i\frac{\Gamma_m^L[1-f_L(E)]+\Gamma_m^R[1-f_R(E)]}{(E-\varepsilon_m)^2+(\Gamma_m/2)^2}. \tag{12}$$

Here $\Gamma_m^K\equiv 2\pi\sum_{k\in K}|V_{mk}|^2\delta(E-\varepsilon_k)$ $(m=g,x,\ K=L,R)$ is electron escape rate from level m into contact K, $\Gamma_m=\Gamma_m^L+\Gamma_m^R$, $f_K(E)$ is the Fermi-Dirac thermal distribution in contact $K=L,R$.

For the evaluation of the phonon Green functions, we again disregard the molecule-radiation field coupling, but keep the electron-phonon interaction. This leads to

$$D^r(\omega)=\Big[\big[D_0^r(\omega)\big]^{-1}-\Pi_{th}^r(\omega)-\Pi_{el}^r(\omega)\Big]^{-1}, \tag{13}$$

$$D^{>/<}(\omega)=D^r(\omega)\Big(\Pi_{th}^{>/<}(\omega)+\Pi_{el}^{>/<}(\omega)\Big)D^a(\omega). \tag{14}$$

We will henceforth assume that $\omega>0$ and use $D^{>/<}(-\omega)=D^{</>}(\omega)$ to access the $\omega<0$ region. In Eqs. (13) and (14) $D^a(\omega)=[D^r(\omega)]^*$,

$$D_0^r(\omega)=\frac{1}{\omega-\omega_v+i\delta}-\frac{1}{\omega+\omega_v+i\delta} \tag{15}$$

is the retarded projection of free phonon Green function, and

$$\Pi_{th}^r(\omega)=-i\frac{\gamma(\omega)}{2}, \tag{16}$$
$$\Pi_{th}^{<}(\omega)=-i\gamma(\omega)N(\omega), \tag{17}$$
$$\Pi_{th}^{>}(\omega)=-i\gamma(\omega)[1+N(\omega)] \tag{18}$$

are the projections of the self-energy of the molecular vibration due to its coupling to the (bosonic) white thermal bath. Here $N(\omega)$ is the Bose-Einstein thermal distribution and $\gamma(\omega)=2\pi\sum_\beta\left|V_\beta^{th}\right|^2\delta(\omega-\omega_\beta)$ is the dissipation rate of molecular vibrational excitation due to coupling to thermal bath. The self-energy of the molecular phonon associated with the electron-vibration coupling is treated at the level of the Born approximation,

$$\Pi_{el}^r(\omega)=-iM_g^2\int\frac{dE}{2\pi}\Big(G_g^{<}(E)\,G_g^a(E-\omega)+G_g^r(E)\,G_g^{<}(E-\omega)\Big), \tag{19}$$
$$\Pi_{el}^{<}(\omega)=-iM_g^2\int\frac{dE}{2\pi}\,G_g^{<}(E)\,G_g^{>}(E-\omega), \tag{20}$$
$$\Pi_{el}^{>}(\omega)=-iM_g^2\int\frac{dE}{2\pi}\,G_g^{>}(E)\,G_g^{<}(E-\omega). \tag{21}$$

Before describing our numerical results, it is important to note the different physical origins of the four contributions, Eqs. (7a)-(7d), to the Raman signal, that can be inferred from the different forms of the electronic Green functions appearing in them and the forms of the corresponding energy denominators.[33] This is most readily recognized by considering these terms in the absence of the vibrational Raman shift. The contribution (7a) with the Green functions product $G_g^{<}G_g^{<}G_x^{>}G_x^{>}$ corresponds to the scattering amplitude involving electronic excitation from occupied electronic level near E_g to empty electronic level near E_x (in the absence of vibrational shift this corresponds to Rayleigh

scattering). Similarly, the contribution (7b) with $G_g^< G_g^> G_x^> G_x^>$ corresponds to electronic Raman scattering that leaves behind an electronic excitation between two metal levels with energies close to E_g. The term (7c) with $G_g^< G_g^< G_x^< G_x^>$ is similar, except that the scattering involves electron motion between two levels near E_x. Finally, the contribution (7d) with $G_g^< G_g^> G_x^< G_x^>$, if considered without the vibrational shift, corresponds to the Raman scattering by two electronic excitations between four metal levels with energies near E_g (two levels, one occupied and the other empty) and E_x (the other two levels, again one occupied and the other empty).

Two observations follow, still on this qualitative level: First, in equilibrium and at low bias, in the common situation where the lower and upper electronic orbitals are far below and far above the metal(s) Fermi energy(ies) respectively, Eq. (7a) will be the dominant contribution to the vibrational Raman signal. Second, the vibrational Raman lines associated with this contribution will be narrow in the sense that their width will not reflect the excitation of electron-hole pairs in the metal. The contributions (7b) and (7c) will be important in situations where, respectively, E_g and E_x are close to the metal Fermi energies. Furthermore, these contributions will be considerably broader, reflecting the excitation of electron-hole pairs in the metal alongside the vibrational excitation. Note that at low temperatures this broadening will be asymmetric, corresponding to an electronic side-band of the vibrational Raman transition as recently discussed in Ref. 16. Finally, we expect that also the pure vibrational Raman spectrum associated with Eq. (7a) will be broader when one of the molecular electronic levels is close to the Fermi energy, because of the increased importance of the electronic relaxation channel for the molecular vibration in this situation.[23]

III. NUMERICAL RESULTS

Here we present numerical results for the Raman flux, Eq. (7), for the model (1)-(4). Below we focus on the most prominent contributions, Eqs. (7a) and (7b). The following parameters are used in these calculations: $T = 100$ K, $\varepsilon_x - \varepsilon_g = 2$ eV (the absolute level positions are varied as described below), $\Gamma_m^L = \Gamma_m^R = 0.05$ eV (in Figs. 2 and 4) and 0.4 eV (in Figs. 3 and 5), $(m = g, x)$, $\omega_v = 0.2$ eV, $\gamma(\omega_v) = 10^{-3}$ eV, and $M_g = 0.03$ eV. The Fermi energy is chosen as the origin, $E_F = 0$, and the bias is applied symmetrically $\mu_L = E_F + |e|V_{sd}/2$ and $\mu_R = E_F - |e|V_{sd}/2$. The incident frequency is taken as $\nu_i = 1$ eV, which corresponds for the present choice of molecular parameters to off-resonant Raman scattering. The couplings to the radiation field are assumed to satisfy $U_{\alpha D}^{(0)} = U_{\alpha D}^{(1)} = 0.01$ eV. The optical resolution windows of the incident energy and measuring device, $\Delta\nu_i$ and $\Delta\nu_f$ in Eq. (7), are taken to be the same, 0.01 eV. The calculations were performed on an energy grid spanning the range from −5 to 5 eV with step size 5×10^{-5} eV.

We envision an experiment in which the position of the molecular resonances can be changed by a gate voltage. We start from the situation where level g is far below the Fermi energy and level x is far above it, so that the lower level is occupied and the upper one is empty, and consider the effect on the Raman spectrum of applying a gate voltage to move ε_g to the vicinity of, and then beyond, the chemical potentials. In this regime the two main contributions to the Raman flux are given by Eqs. (7a) and (7b) with the first one dominating the intensity of the Stokes line. (As explained above, the terms (7c) and (7d) are potentially important only when the excited state is populated). The Raman linewidths reported below are estimated using the standard deviation associated with

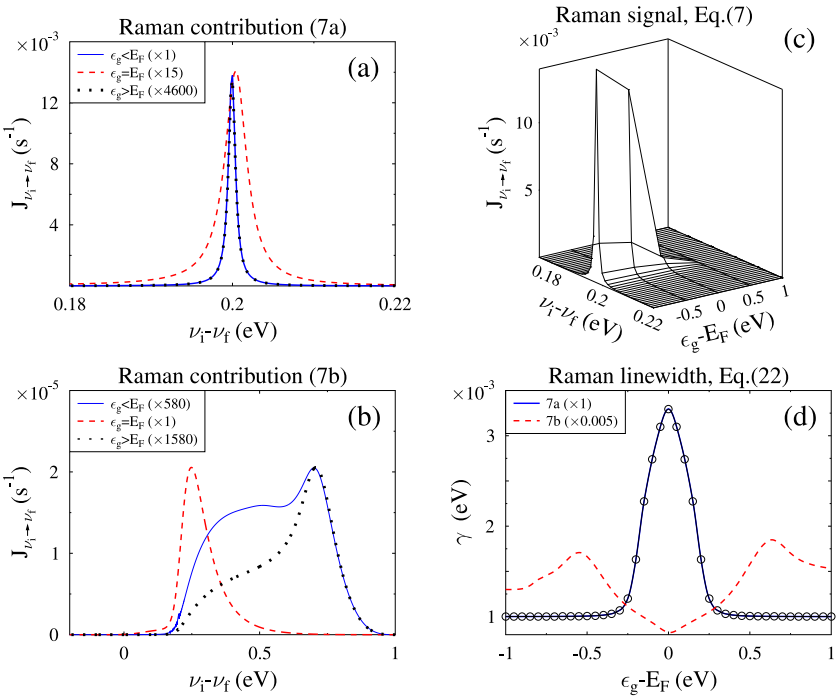

FIG. 2. The Stokes component of the vibrational Raman scattering at equilibrium, $\mu_L = \mu_R = E_F$, for weak molecule-contacts coupling, $\Gamma_m^K = 0.05$ eV. See text for parameters.

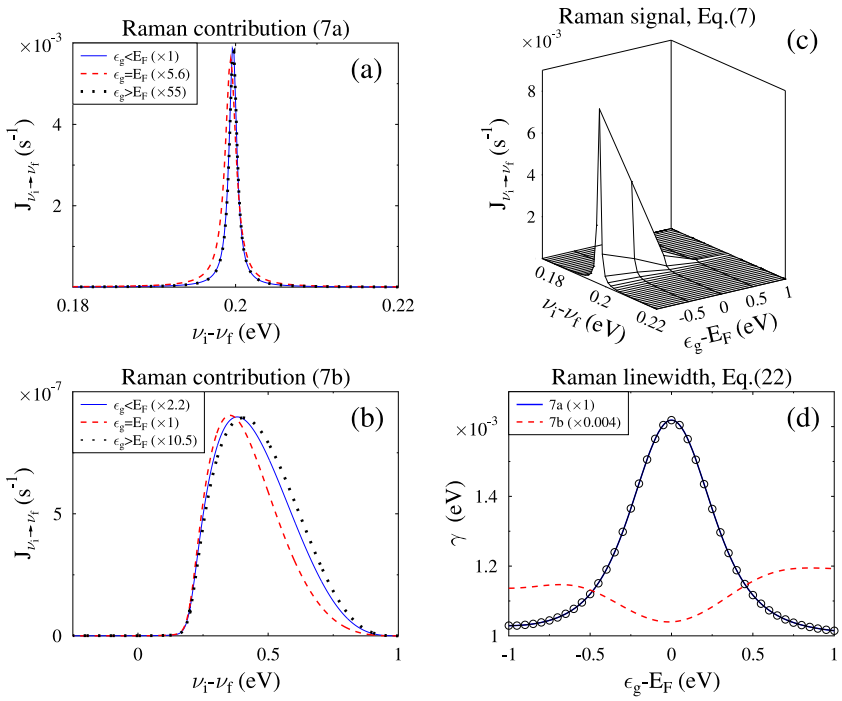

FIG. 3. The Stokes component of the vibrational Raman scattering at equilibrium, $\mu_L = \mu_R = E_F$, for strong molecule-contacts coupling, $\Gamma_m^K = 0.4$ eV. See text for parameters.

the corresponding Raman peak calculated on the employed energy grid (see Eqs. (22) and (23) below).

Figures 2 and 3 show results of this calculation for the equilibrium case, $\mu_L = \mu_R = E_F$, for weak $\Gamma_m^K = 0.05$ eV and strong $\Gamma_m^K = 0.4$ eV molecule-contacts coupling. Panels (a) and (b) of these figures show two main contributions to the vibrational Raman signal $J_{\nu_i\to\nu_f}$, Eqs. (7a) and (7b), vs. the Raman shift $\nu_i - \nu_f$ for three different positions of electronic level ε_g: below ($\varepsilon_g - E_F = -0.5$ eV, solid line, blue), at ($\varepsilon_g - E_F = 0$, dashed line, red), and above ($\varepsilon_g - E_F = 0.5$ eV, dotted line, black) the Fermi energy. Panel (c) presents the map of the total Raman signal vs. Raman shift $\nu_i - \nu_f$ and the level position relative to the Fermi energy $\varepsilon_g - E_F$. Finally, panel (d) shows widths γ of the two main contributions to the Stokes Raman scattering (Eq. (7a)—solid line, blue; Eq. (7b)—dashed line, red) as function of the lower level position relative to the Fermi energy $\varepsilon_g - E_F$. The widths are calculated according to

$$\gamma = \sqrt{\overline{\nu_{if}^2} - \left(\overline{\nu}_{if}\right)^2}, \tag{22}$$

where

$$\overline{\nu_{if}^n} = \int_0^\infty d(\nu_i - \nu_f) J_{\nu_i\to\nu_f}(\nu_i - \nu_f)^n. \tag{23}$$

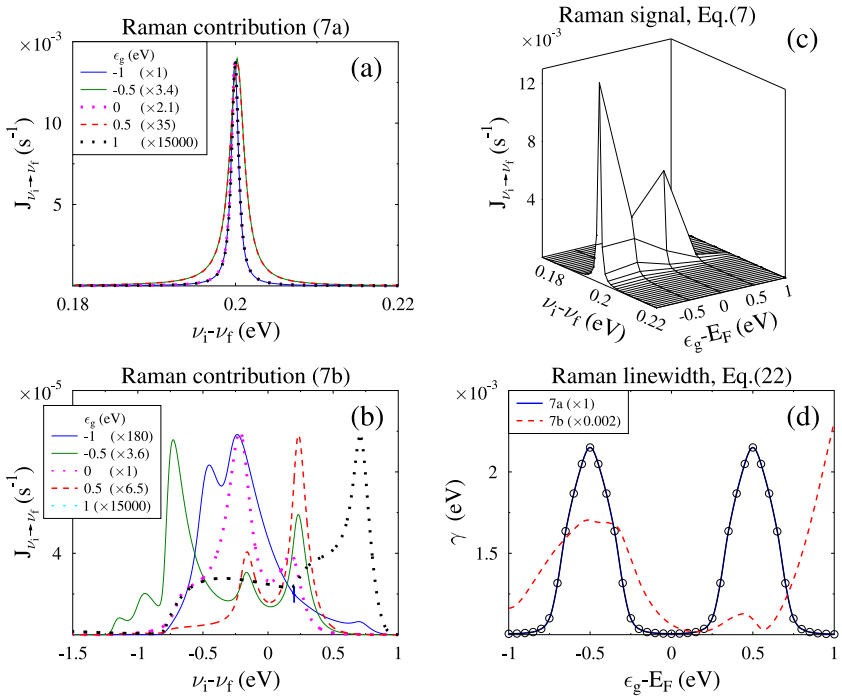

FIG. 4. Stokes scattering from a biased junction, $\mu_L = 0.5$ eV and $\mu_R = -0.5$ eV for weak molecule-contacts coupling, $\Gamma_m^K = 0.05$ eV. See text for parameters.

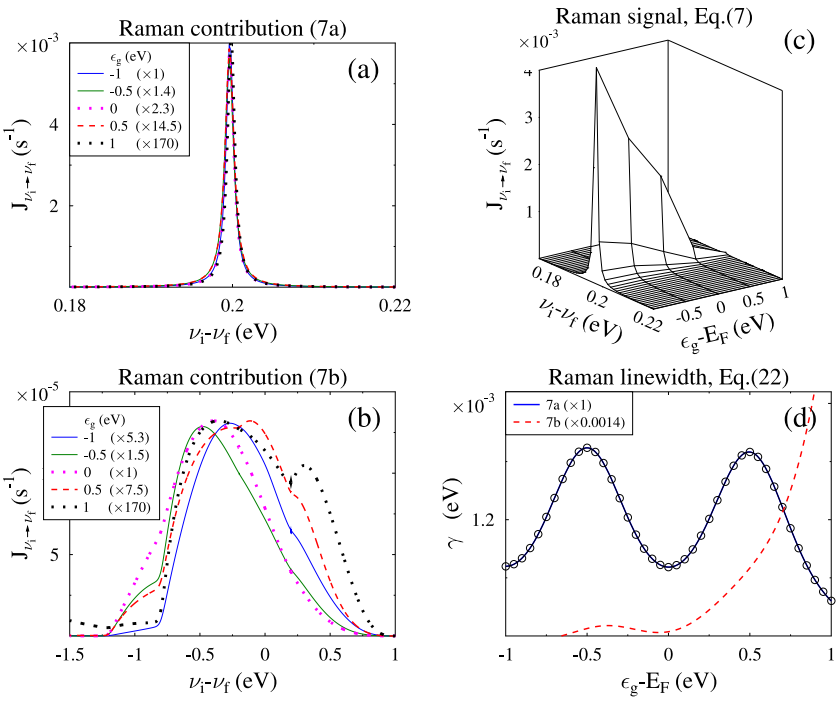

FIG. 5. Stokes scattering from a biased junction, $\mu_L = 0.5$ eV and $\mu_R = -0.5$ eV, for strong molecule-contacts coupling, $\Gamma_m^K = 0.4$ eV. See text for parameters.

Circles in panel (d) indicate the broadening of the molecular vibration due to coupling to electron-hole excitations, calculated from $-\mathrm{Im}\, D^r(\nu_i - \nu_f)$, Eq. (13). Note that the intensity of the Stokes line decreases with decrease of the population in the ground state (see Fig. 2(c)), however the implication of this observation should be understood with respect to the 2-level model used here. In reality, when ε_g goes up and above the metal Fermi energy, other lower molecular levels will contribute to the Raman signal. Disregarding this issue, the following additional observations can be made:

1. The dominant Raman feature is indeed that associated with contribution (7a) the electronically elastic/vibrationally inelastic signal. The contribution (7b) becomes comparable when ε_g is near the metal Fermi energy. It should be kept in mind that and additional broad feature, the electronically inelastic/vibrationally elastic (pure electronic) is not displayed in these figures. In experimental spectra, the signal (7b) may often become part of this broad electronic background.
2. The width of the contribution (7b) is far greater than that of the electronically elastic term (7a), as long as ε_g is far from the metal Fermi energy. However, the width of (7a) increases considerably when ε_g approaches E_F.
3. The widths of the two contributions, (7a) and (7b), behave symmetrically about the Fermi energy (see Figs. 2(a) and 2(b)). Such behavior is expected since in both cases the width is defined by convolution of electron and hole populations, $G_g^<(E_{g1})\, G_g^>(E_{g2})$, which at equilibrium is symmetric relative to the Fermi energy.
4. Comparing the results displayed in Figures 2 and 3 (small and large molecule-metal coupling (Γ), respectively), we note that the dominant low bias feature, namely the contribution (7a) is essentially the same in both cases. Interestingly, when ε_g is at the Fermi energy (dashed red lines in Figs. 2(a) and 3(a)), this feature is broader in the smaller Γ case. This is also seen in comparing Figs. 2(d) and 3(d). This behavior reflects the fact that when $\Gamma > k_B T$, even when $\varepsilon_g = E_F$, most of the electronic spectral density (of width Γ) is outside the region of partial electronic occupation ($f(1-f) \neq 0$ where f is the Fermi distribution) in which the electronic channel for vibrational relaxation is open. The fact that the spectra in Fig. 3 are smoother and less structured than in Fig. 2 similarly reflects the fact that for large Γ all behaviors associated with the position of ε_g relative to E_F and the width of the partially populated region are smoothened.

The width of the vibrational Raman lines reflects three types of contributions. First there is the relaxation to the thermal bosonic environment that is not affected (in our model) by the bias and gate potentials. Second is the additional relaxation channel due to electron-vibration coupling, that can dominate the overall width when the molecular electronic level approaches the metal Fermi level. The structure of this contribution suggests that the width of the term (7a) (solid line in Fig. 2(d)) is dominated by the (renormalized) density of molecular vibration (circles in Fig. 2(d)). Finally, as discussed above, there is the electron-hole sideband that appears prominently in the term (7b) (as well as (7c) and (7d)). Note again that in actual observations it will not be easy to distinguish between this sideband to the vibrational transition and the underlying Raman continuum that originates primarily from the pure electronic Raman scattering.[11]

We now turn to the nonequilibrium situation with $\mu_L = 0.5$ eV and $\mu_R = -0.5$ eV. Figures 4 and 5 are nonequilibrium analogs of Figures 2 and 3, respectively. Here panels (a) and (b) present results for the two main

contributions, Eqs. (7a) and (7b), at five positions of level ε_g relative to electrochemical potentials of the contacts μ_L and μ_R: $\varepsilon_g < \mu_R$ ($\varepsilon_g = -1$ eV, solid line, blue), $\varepsilon_g = \mu_R$ (solid line, green), $\mu_R < \varepsilon_g < \mu_L$ ($\varepsilon_g = 0$, dotted line, magenta), $\varepsilon_g = \mu_L$ (dashed line, red), and $\varepsilon_g > \mu_L$ ($\varepsilon_g = 1$ eV, dotted line, black). As previously, panel (c) shows the total Stokes scattering, Eq. (5), as a function of the Raman shift and level position; panel (d) presents Raman linewidths γ, Eq. (22) of the two main contributions (Eq. (7a)—solid line, blue; Eq. (7b)—dashed line, red) as functions of the level position. Circles in panel (d) indicate the broadening of the molecular vibration due to coupling to electron-hole excitations, calculated from $-\mathrm{Im}\, D^r(\nu_i - \nu_f)$, Eq. (13).

Here the total Stokes intensity is affected by two factors: the population of the lower level and the current induced heating of the molecular vibration. As a result, the decrease in the Stokes intensity when ε_g approaches the lowest chemical potential due to depletion of the level population changes to increase in the intensity when the level is in the bias window (nonequilibrium feature)—see Fig. 4(c). The width of the dominant contribution (7a) shows similar behavior as in the equilibrium case, with increase of the width resulting from opening the electronic relaxation channel when ε_g approaches the metal Fermi energies. This contribution to the width is again symmetric about each of the Fermi energies (see Figs. 4(d) and 5(d)). In contrast, the nonequilibrium electronic distribution, in particular the existence of two energy regions of partial populations of metal electronic states, causes drastic changes and more structure in both lineshape (Fig. 4(b)) and linewidth (Fig. 4(d)) of the contribution (7b) as compared to equilibrium case. This structure is again smoothened in the large Γ case (Fig. 5). Still, since this peak is much lower and broader than that of (7a), it may be considered as part of the electronic Raman background.

IV. CONCLUSION

Within a simple two-level model of a molecular junction we consider off-resonant Raman scattering and discuss dependence of Stokes linewidth on gate and bias voltages. We focus on low bias regime, where upper level is almost empty, and thus consider only "normal Raman" contribution to the total signal (i.e., Raman scattering which originates at the lower molecular level). Employing realistic parameters we show that the linewidth changes non-monotonically with gate voltage demonstrating maximum at resonance between molecular level and chemical potential(s) of metallic contacts. Analysis shows that the effect is due to opening of an electronic relaxation channel for molecular vibrations by which e-h excitations are formed in metallic contacts. At low biases and for realistic parameters this mechanism is the dominant contribution to the Stokes linewidth. Other mechanisms are relaxation of molecular vibration due to coupling to the thermal environment and surface plasmons. The latter was not included in the consideration due to mismatch between characteristic plasmons and molecular vibration frequencies. Note that the model also disregards inhomogeneous broadening and pure dephasing contributions. Experimental verification of our theoretical prediction seems to be a realistic possibility.

ACKNOWLEDGMENTS

The research of A.N. is partially supported by the Israel Science Foundation and the US-Israel Binational Science Foundation. M.G. gratefully acknowledges support by the US Department of Energy.

APPENDIX: ELECTRON AND PHONON GREEN FUNCTIONS

General definitions of electron G and phonon D Green functions (GFs) on the Keldysh contour are[34]

$$G_{m_1m_2}(\tau_1,\tau_2) = -i\langle T_c\, \hat{d}_{m_1}(\tau_1)\, \hat{d}^\dagger_{m_2}(\tau_2)\rangle, \tag{A1}$$

$$D_{v_1v_2}(\tau_1,\tau_2) = -i\langle T_c\, \hat{Q}_{v_1}(\tau_1)\, \hat{Q}^\dagger_{v_2}(\tau_2)\rangle, \tag{A2}$$

where $\tau_{1,2}$ are contour variables and T_c is contour ordering operator, operators are presented in the Heisenberg picture and $\langle \ldots \rangle = \mathrm{Tr}[\ldots \hat{\rho}_0]$ is quantum mechanical and statistical averaging with respect to original density operator $\hat{\rho}_0$ of the whole system. In our treatment we retain only diagonal elements of the GFs due to assumption $\varepsilon_x - \varepsilon_g \ll \Gamma_{x,g}$ for the electron GF and only one vibrational mode considered in the model for the phonon GF. This leads to definitions presented in Eqs. (8) and (9).

The GFs satisfy the Dyson equations

$$\mathbf{G}(\tau_1,\tau_2) = \mathbf{G}_0(\tau_1,\tau_2) + \int_c d\tau_3 \int_c d\tau_4\, \mathbf{G}_0(\tau_1,\tau_3) \times \Sigma(\tau_3,\tau_4)\, \mathbf{G}(\tau_4,\tau_2), \tag{A3}$$

$$\mathbf{D}(\tau_1,\tau_2) = \mathbf{D}_0(\tau_1,\tau_2) + \int_c d\tau_3 \int_c d\tau_4\, \mathbf{D}_0(\tau_1,\tau_3) \times \Pi(\tau_3,\tau_4)\, \mathbf{D}(\tau_4,\tau_2), \tag{A4}$$

where $\int_c \ldots$ is on-the-contour integration, GFs are assumed to be matrices (in electron and phonon subspaces, respectively), Σ and Π are electron and phonon self-energies representing the effect of other system degrees of freedom on electrons and phonons, and $\mathbf{G}_0$ and $\mathbf{D}_0$ are free GFs, i.e., GFs for isolated electrons and phonons. In our model this corresponds to disregarding second and third rows of Eq. (2) and Eq. (4). In our treatment we need only retarded projection of the free phonon GF, explicit form of its Fourier transform is given in Eq. (15).[35] Projections of the Dyson equation (A4) are presented in Eqs. (13) and (14).

In the model self-energy Σ consists of contributions due to molecule-contacts coupling (fourth term in Eq. (2)), electron-phonon interaction (fifth term in Eq. (2)), and field-matter interaction, Eq. (4). Assuming that molecule-contacts coupling is the strongest interaction, we disregard the other two contributions in treating electron GFs. Self-energy for molecular coupling to the contacts is known exactly[34]

$$\Sigma^K_{m_3m_4}(\tau_3,\tau_4) = \sum_{k\in K} V_{m_3k}\, g_k(\tau_3,\tau_4)\, V_{km_4}. \tag{A5}$$

Here $g_k(\tau_3,\tau_4)$ is the GF of the free electron in state k of contact K (L or R). The Fourier transform of its retarded

projection

$$\Sigma^{K\,r}_{m_3m_4}(E) = \sum_{k\in K} \frac{V_{m_3k}V_{km_4}}{E-\varepsilon_k+i\delta} \equiv \Lambda^K_{m_3m_4}(E) - \frac{i}{2}\Gamma^K_{m_3m_4}(E) \tag{A6}$$

accounts for the Lamb shift Λ and dissipation Γ of molecular levels due to coupling to contact K. In the wide-band approximation[36] the former is disregarded, while the latter is assumed to be energy independent. Its lesser and greater projections[34]

$$\Sigma^{K<}_{m_3m_4}(E) = i\Gamma^K_{m_3m_4}f_K(E), \tag{A7}$$

$$\Sigma^{K>}_{m_3m_4}(E) = -i\Gamma^K_{m_3m_4}[1-f_K(E)], \tag{A8}$$

yield information on occupied and empty states in the contact. Here $f_K(E)$ is the Fermi-Dirac distribution.

In the model the two levels (ε_g and ε_x) represent HOMO and (effective) LUMO. In molecules separation between these levels is of the order of several eV. Taking into account that usual molecule-contacts coupling strength is of the order 0.01–0.1 eV, hybridization between these levels (induced by the off-diagonal matrix elements of $\Gamma^K_{m_3m_4}$) is negligible. Utilizing diagonal terms of (A6)-(A8) in projections of the Dyson equation (A3) leads to Eqs. (10)-(12). Retarded, lesser, and greater projections of electron GFs yield information on molecular subspace electron spectral density, its occupied and empty states, respectively.

Phonon self-energy Π has contributions from electron-phonon interaction and coupling to the thermal bath, last two terms of Eq. (2) - $\Pi = \Pi_{el} + \Pi_{th}$. The latter is known exactly[14]

$$P_{th}(\tau_3,\tau_4) = \sum_\beta |V^{th}_\beta|^2 d_\beta(\tau_3,\tau_4), \tag{A9}$$

where $d_\beta(\tau_3,\tau_4)$ is the GF of free phonons in the thermal bath. Fourier transforms of its retarded, lesser, and greater projections are given in Eqs. (16)-(18).

Phonon self-energy due to electron-phonon interaction can be evaluated only approximately. Following standard diagrammatic procedure[14] and employing the lowest (second) order in electron-phonon interaction yields

$$\Pi_{el}(\tau_3,\tau_4) = -i\sum_{m_3,m_4} M_{m_3}\,G_{m_3m_4}(\tau_3,\tau_4)\,G_{m_4m_3}(\tau_4,\tau_3)\,M_{m_4}. \tag{A10}$$

Fourier transforms of retarded, lesser, and greater projections of this expression are given in Eqs. (19)-(21). Here we employed Eqs. (10)-(12) for the electron GFs.

[1]M. Galperin and A. Nitzan, Phys. Chem. Chem. Phys. **14**, 9421 (2012).
[2]S. W. Wu, G. V. Nazin, and W. Ho, Phys. Rev. B **77**, 205430 (2008).
[3]C. Chen, P. Chu, C. A. Bobisch, D. L. Mills, and W. Ho, Phys. Rev. Lett. **105**, 217402 (2010).
[4]N. L. Schneider, G. Schull, and R. Berndt, Phys. Rev. Lett. **105**, 026601 (2010).
[5]N. L. Schneider, J. T. Lü, M. Brandbyge, and R. Berndt, Phys. Rev. Lett. **109**, 186601 (2012).
[6]C. Grosse, M. Etzkorn, K. Kuhnke, S. Loth, and K. Kern, Appl. Phys. Lett. **103**, 183108 (2013).
[7]Z. Ioffe, T. Shamai, A. Ophir, G. Noy, I. Yutsis, K. Kfir, O. Cheshnovsky, and Y. Selzer, Nat. Nanotechnol. **3**, 727 (2008).
[8]D. R. Ward, N. J. Halas, J. W. Ciszek, J. M. Tour, Y. Wu, P. Nordlander, and D. Natelson, Nano Lett. **8**, 919 (2008).
[9]D. R. Ward, D. A. Corley, J. M. Tour, and D. Natelson, Nat. Nanotechnol. **6**, 33 (2011).
[10]M. Galperin and A. Nitzan, J. Phys. Chem. Lett. **2**, 2110 (2011).
[11]M. Galperin and A. Nitzan, Phys. Rev. B **84**, 195325 (2011).
[12]Y. Selzer and U. Peskin, J. Phys. Chem. C **117**, 22369 (2013).
[13]M. A. Ochoa, Y. Selzer, U. Peskin, and M. Galperin, J. Phys. Chem. Lett. **6**, 470 (2015).
[14]M. Galperin, M. A. Ratner, and A. Nitzan, J. Chem. Phys. **121**, 11965 (2004).
[15]D. Rai and M. Galperin, Phys. Rev. B **86**, 045420 (2012).
[16]S. Dey, M. Banik, E. Hulkko, K. Rodriguez, V. A. Apkarian, M. Galperin, and A. Nitzan, Phys. Rev. B **93**, 035411 (2016).
[17]H. Park, J. Park, A. K. L. Lim, E. H. Anderson, A. P. Alivisatos, and P. L. McEuen, Nature **407**, 57 (2000).
[18]A. N. Pasupathy, J. Park, C. Chang, A. V. Soldatov, S. Lebedkin, R. C. Bialczak, J. E. Grose, L. A. K. Donev, J. P. Sethna, D. C. Ralph, and P. L. McEuen, Nano Lett. **5**, 203 (2005).
[19]D.-H. Chae, J. F. Berry, S. Jung, F. A. Cotton, C. A. Murillo, and Z. Yao, Nano Lett. **6**, 165 (2006).
[20]M. Galperin, A. Nitzan, and M. A. Ratner, Phys. Rev. B **78**, 125320 (2008).
[21]A. J. White and M. Galperin, Phys. Chem. Chem. Phys. **14**, 13809 (2012).
[22]D. Natelson, Y. Li, and J. B. Herzog, Phys. Chem. Chem. Phys. **15**, 5262 (2013).
[23]K. Kaasbjerg, T. Novotný, and A. Nitzan, Phys. Rev. B **88**, 201405 (2013).
[24]Y. Li, P. Doak, L. Kronik, J. B. Neaton, and D. Natelson, Proc. Natl. Acad. Sci. U. S. A. **111**, 1282 (2014).
[25]A. J. White, S. Tretiak, and M. Galperin, Nano Lett. **14**, 699 (2014).
[26]A. J. White, M. A. Ochoa, and M. Galperin, J. Phys. Chem. C **118**, 11159 (2014).
[27]W. Wang, T. Lee, I. Kretzschmar, and M. A. Reed, Nano Lett. **4**, 643–646 (2004).
[28]M. Galperin, M. A. Ratner, and A. Nitzan, Nano Lett. **4**, 1605 (2004).
[29]In molecules Raman scattering will involve a set of excited states, which for the off-resonant scattering can be effectively represented by a single level ε_x. This is in similarity to effective couplings introduced in problems involving super-exchange electron transfer between donor and acceptor mediated by a bridge.
[30]M. Galperin, M. A. Ratner, and A. Nitzan, Nano Lett. **9**, 758 (2009).
[31]M. Galperin, M. A. Ratner, and A. Nitzan, J. Chem. Phys. **130**, 144109 (2009).
[32]For strongly biased junctions both lower and upper molecular states may be partially occupied, giving rise to more contributions to elastic and inelastic light scattering, see Ref. 31.
[33]It is convenient to look at them in comparison to the pure electronic Raman components discussed in Ref. 11 (see Fig. 2 in this reference).
[34]H. Haug and A.-P. Jauho, *Quantum Kinetics in Transport and Optics of Semiconductors*, 2nd ed. (Springer, Berlin, Heidelberg, 2008), substantially revised edition.
[35]G. D. Mahan, *Many-Particle Physics* (Plenum Press, 1990).
[36]G. Stefanucci and R. van Leeuwen, *Nonequilibrium Many-Body Theory of Quantum Systems: A Modern Introduction* (Cambridge University Press, 2013).